Biogeosciences Discuss., doi:10.5194/bg-2016-112, 2016
Manuscript under review for journal Biogeosciences
Published: 5 April 2016

Biogeosciences Discussions Open Access EGU

Drivers of Multicentury Trends in the Atmospheric CO_2 Mean Annual Cycle in a Prognostic ESM

Jessica Liptak[1], Gretchen Keppel-Aleks[1], and Keith Lindsay[2]

[1]Department of Climate and Space Sciences and Engineering, University of Michigan, Ann Arbor, MI, USA
[2]Climate and Global Dynamics, National Center for Atmospheric Research, Boulder, CO, USA

Correspondence to: Jessica Liptak (liptak@umich.edu)

Abstract. The amplitude of the mean annual cycle of atmospheric CO_2 has increased by at least 0.5% yr^{-1} over most of the Northern Hemisphere (NH) extratropics during the last three decades likely from a combination of enhanced atmospheric CO_2, climate change, and anthropogenic land use change. We investigated how each of these factors affected the increase in the atmospheric CO_2 mean annual cycle amplitude simulated by the Community Earth System Model (CESM), a prognostic coupled climate-carbon cycle model. The simulated amplitude of the NH mean CO_2 annual cycle showed a weaker trend than observed, increasing by only 15% over the period spanning 1950–2010. By 2100, the amplitude rose to 57% above the present-day baseline (1950–1959), and reached a maximum of 76% above the baseline around 2250.

The amplitude increase in the CESM was mainly driven by climate change and changing atmospheric composition, with the largest amplitude gains occurring in the mid- and high latitudes. In addition, the long-term simulations revealed shifts in key climate drivers of the atmospheric CO_2 seasonality that were not apparent before 2100. Climate change from NH boreal ecosystems was the largest driver of Arctic CO_2 annual cycle amplification between 1950 and 2100. CO_2 fertilization and nitrogen deposition in the NH boreal and temperate ecosystems contributed the most to the amplitude increase over the midlatitudes through 2300 and over the Arctic after 2100. Greater terrestrial productivity during the growing season contributed the most to the annual cycle amplification over the high latitudes, midlatitudes, and the NH tropics, reflecting lengthening of the growing season rather than the strength of the terrestrial carbon sink. Prior to 2100, CO_2 annual cycle amplification occurred in conjunction with an increase in the NH land carbon sink, but the trends decoupled after 2100, underscoring that an increasing atmospheric CO_2 annual cycle amplitude is not predicated on a strengthened terrestrial carbon sink.

1 Introduction

The amplitude of the mean annual cycle of atmospheric CO_2, an indicator of the seasonal cycle of terrestrial and ocean carbon exchange, has increased over the Northern Hemisphere (NH) since observational records began in the late 1950s (Pearman and Hyson, 1981; Cleveland et al., 1983; Bacastow et al., 1985; Conway et al., 1994; Keeling et al., 1996; Randerson et al., 1997; Graven et al., 2013; Liu et al., 2015). The largest increases of 40–50% were inferred over the northern high latitudes from surface observations (Keeling et al., 1996) and from aircraft observations of the free troposphere (Graven et al., 2013). The isotopic composition of CO_2 indicates that the amplification of the atmospheric CO_2 annual cycle reflects enhanced net exchange

Biogeosciences Discuss., doi:10.5194/bg-2016-112, 2016
Manuscript under review for journal Biogeosciences
Published: 5 April 2016

of CO_2 between the atmosphere and the land rather than the ocean (Manning, 1993). Land-atmosphere CO_2 exchange is highly seasonal, especially in the NH mid- and high latitudes where photosynthesis draws down CO_2 in the spring and summer, and net ecosystem respiration returns CO_2 to the atmosphere (e.g., Komhyr et al., 1985; Enting and Mansbridge, 1989; Nemry et al., 1996; Dettinger and Ghil, 1998).

Recent work has identified several plausible drivers of the increasing mean annual cycle amplitude, although a full accounting of the trend remains elusive. Direct anthropogenic impacts on the mean annual cycle amplitude include changing patterns of fossil fuel emissions and land use. NH fossil fuel CO_2 emissions generally peak during winter when heating is required, enhancing the mean annual cycle from biospheric fluxes. Increasing fossil fuel emissions from 6 major industrial regions across the globe (Rotty, 1987), however, were shown to contribute less than 1% yr^{-1} to the trend in the NH CO_2 annual cycle amplitude (Randerson et al., 1997).

Responses to changing environmental conditions likely represent another important driver for increases to the CO_2 mean annual cycle (Graven et al., 2013; Zeng et al., 2014). The magnitude of the amplitude increase indicates a dominant role for enhanced GPP during the growing season in addition to increased CO_2 release during the dormant season (Graven et al., 2013). More recently, agricultural intensification, including irrigation and fertilization of agricultural land, has been suggested to cause significant increases in the CO_2 amplitude by increasing carbon uptake during the summer growing season (Gray et al., 2014; Zeng et al., 2014). For example, Gray et al. (2014) found that enhanced summer growing season carbon uptake by midlatitude cropland contributed 17–25% (1.4 Pg C yr^{-1}) to the 1961–2008 NH extratropical CO_2 annual cycle amplitude trend. Zeng et al. (2014) likewise identified high-latitude natural vegetation and midlatitude crops as the largest contributors to the 1961–2010 NH annual cycle amplitude trend.

Changing atmospheric composition from increased CO_2 and anthropogenic nitrogen is another potential driver of enhanced terrestrial productivity. Greater atmospheric CO_2 may facilitate plant carbon uptake through increased water use efficiency (Keenan et al., 2013), and results from Kohlmaier et al. (1989) and McGuire et al. (2001) suggest that CO_2 fertilization adds at least 10% to the CO_2 mean annual cycle amplitude trend. The availability of nitrogen in the soil limits terrestrial productivity (Vitousek and Howarth, 1991) and, therefore, constrains the effects CO_2 fertilization on GPP as the demand for nitrogen increases (Luo et al., 2004). However, emission of nitrogen oxides (NO_x) and ammonia from combustion, livestock, agriculture, and industrial sources may augment the supply of soil nitrogen available for fixation by plants (Prentice et al., 2001).

Climate change-induced warming during the growing season and lengthening of the growing season present another pathway through which GPP may be stimulated. Keeling et al. (1996) proposed that increased terrestrial CO_2 uptake from a longer high latitude growing season has driven the amplification of the CO_2 annual cycle, since the trends in the CO_2 annual cycle amplitude strengthen moving northward, and the greatest warming has occurred during the winter and spring over the northern high latitudes. Findings by Randerson et al. (1999), McDonald et al. (2004), Barichivich et al. (2013) support the hypothesis that longer growing seasons enhance spring CO_2 uptake and annual cycle amplitudes over the Arctic. This effect may be counteracted by the fact that growth during the spring over northern mid- and high latitudes may cause growing season moisture deficits that reduce terrestrial productivity later in the growing season (Angert et al., 2005; Buermann et al., 2013; Parida and Buermann, 2014). The combined effects of climate change and shifts in vegetation cover in simulations can also

Biogeosciences Discuss., doi:10.5194/bg-2016-112, 2016
Manuscript under review for journal Biogeosciences
Published: 5 April 2016

enhance GPP. Forkel et al. (2016) showed that the interaction of vegetation dynamics and climate change lead to greater GPP over NH boreal and Arctic regions that, in turn, drove the observed increases in NH high latitude seasonal CO_2 amplitudes.

Disturbance may also contribute to the amplification of the NH CO_2 annual cycle. Fire contributes less than 10% to the NH mid- and high latitude CO_2 annual cycle amplitudes, and hence only a small percentage to the NH annual cycle amplification (Randerson et al., 1997; Wittenberg et al., 1998), but can have a large local impact on productivity. Zimov et al. (1999) showed that seasonal amplitudes of net ecosystem exchange (NEE) were 2–3.5 times greater at Siberian sites disturbed by grazing and fire than at undisturbed sites. Similarly, Welp et al. (2006) found that the CO_2 annual cycle amplitude was larger, despite the growing season starting 3 weeks later and lasting 7 fewer weeks, over a 15-year old previously-burned tree stand than an 80-year old stand.

In short, there are several potential drivers of the CO_2 annual cycle amplification that feed back onto the climate system and create large uncertainty surrounding the future behavior of the terrestrial carbon cycle. Earth System models (ESMs) make it possible to study long-term effects natural and anthropogenic forcing on the terrestrial carbon cycle. Unlike empirical models, ESMs provide mechanistic representations of the carbon cycle by coupling land surface models that explicitly solve for biogeochemical processes with models of the atmosphere, ocean, and other components of the climate system (Claussen et al., 2002). We used the Community Earth System Model (CESM) to study the contribution of natural drivers of variability in CO_2 fluxes to the increasing amplitude by separating the effects of CO_2 radiative forcing (climate change), CO_2 fertilization and nitrogen deposition from changes in the atmospheric chemical composition, and land use change on the atmospheric CO_2 annual cycle amplitude over the NH subtropics, NH midlatitudes, and the Arctic before and after 2100 in an extension of the high-emissions RCP8.5 scenario (Meinshausen et al., 2011). In addition to revealing potential effects of continued increases in CO_2 emissions, anthropogenic nitrogen, and land use change up to 2100, extending the RCP8.5 scenario to 2300 allowed us to assess the behavior of the mean annual CO_2 cycle in warmer climate following stabilization of atmospheric CO_2 mole fraction, and a shift in the terrestrial biosphere from a CO_2 sink to a source as shown by Randerson et al. (2015).

This paper is organized as follows: First, we discuss the ability of the CESM to capture present-day observed changes in the mean CO_2 annual cycle amplitude throughout the NH. Second, we describe how climate change, changing atmospheric composition, and land use change impact the NH CO_2 annual cycle amplitude in the CESM before and after 2100. Third, we examine how forcing from different regions contributes to the amplitude changes attributed to each driver.

2 Methods

2.1 Model

We analyzed simulations from the Community Earth System model with coupled biogeochemistry (CESM1(BGC); Hurrell et al. (2013)) to explore the role of environmental change on land-atmosphere carbon exchange. The Community Atmosphere Model (CAM, version 4; Neale et al. (2013)) and the Community Land Model (CLM, version 4; Lawrence et al. (2012)) were the most important components for our research, but all components of the model, including physical and biogeochemical ocean processes and sea ice processes were interactive in the model configuration. The CAM4 was run on a $0.94^\circ \times 1.25^\circ$ finite volume

Biogeosciences Discuss., doi:10.5194/bg-2016-112, 2016
Manuscript under review for journal Biogeosciences
Published: 5 April 2016

grid with 26 vertical levels. The model simulated climate conditions, including temperature, precipitation, and humidity that provide important boundary conditions for land biogeochemistry. Moreover, the CAM4 directly simulates three-dimensional transport of atmospheric CO_2, as well as separate CO_2 tracers derived from fossil fuel emissions, land exchange, and ocean exchange.

The CLM4 exchanged fluxes of sensible and latent heat, momentum, moisture, radiation, and terrestrial carbon with the CAM4, and was run at the same horizontal resolution. Biogeochemistry is represented in CLM4 by a prognostic carbon-nitrogen model (CLM4CN, Thornton et al. (2007)) and fire model adapted from the Thonicke et al. (2001) model. We note that important high latitude processes, such as permafrost carbon dynamics, were not simulated in the CLM4, meaning that the model may have underestimated both the seasonal dynamics of soil carbon fluxes and the long-term dynamics of permafrost melt and the subsequent radiative feedback onto the climate system (Koven et al., 2015).

In our analysis, we used the CLM4 net ecosystem productivity (NEP), defined as the difference between gross primary productivity (GPP) and total respiration (autotrophic + heterotrophic) to calculate the atmospheric CO_2 annual cycle amplitudes described in Section 2.3.

2.2 Experiments

Three CESM simulations were run from 1850 to 2300 to separate the effects of climate change, changing atmospheric composition, and land use change. The simulations had identical boundary conditions for CO_2, which was prescribed based on the historical, RCP8.5, and extended (ECP8.5) CO_2 concentrations outlined by Meinshausen et al. (2011). The degree of coupling between CO_2 biogeochemistry and radiative forcing differed across the three runs. In the first simulation, denoted FullyCoupled, the imposed CO_2 was radiatively active, and additional anthropogenic radiative forcing resulted from prescribed CH_4, chlorofluorocarbons, ozone, and aerosols. In this simulation, the increasing CO_2 was also biogeochemically active, meaning it contributed to CO_2 fertilization. Transient land use change (LUC) from agriculture and wood harvest, and land and ocean nitrogen deposition (N-deposition; Lamarque et al. (2010)) were applied through 2100, then held at 2100 values thru 2300. Keppel-Aleks et al. (2013) and Lindsay et al. (2014) provide additional descriptions of the model configuration and analyses of the FullyCoupled simulation during the 20th century. In the second simulation (NoRad), radiative and non-CO_2 atmospheric anthropogenic forcings were fixed at 1850 values, while CO_2 mole fraction, LUC, and N-deposition were prescribed as in FullyCoupled. Randerson et al. (2015) also details the design of the FullyCoupled and NoRad (referred to as "NoCO$_2$Forcing") simulations through 2300. We isolated the impact of climate change on the mean annual CO_2 cycle by taking the difference between the FullyCoupled and NoRad simulations. The third simulation (NoLUC), was configured identically to FullyCoupled with the exception that LUC was held constant at 1850 values; therefore, LUC effects on terrestrial carbon exchange were determined from the difference between FullyCoupled and NoLUC.

Variations in fractional coverage, albedo, nutrient limitations, and surface energy fluxes among trees, grasses, and crops may enhance or oppose the effects of climate change and CO_2 fertilization on the atmospheric CO_2 mean annual cycle amplitude. These plant functional type (PFT)-based changes were approximated by prescribing transient land cover change through 2100 in FullyCoupled and NoRad based on annual fractional transition among primary vegetation, secondary vegetation, pasture

Biogeosciences Discuss., doi:10.5194/bg-2016-112, 2016
Manuscript under review for journal Biogeosciences
Published: 5 April 2016

(grazing land), and crops described by Hurtt et al. (2006). The crop model was inactive in the CESM simulations, and the crop PFT in Hurtt et al. (2006) data was specified as unmanaged grass (Lindsay et al., 2014). Therefore, our CESM results do not include anthropogenic influences such as fossil fuel emissions seasonality or agricultural intensification. Lawrence et al. (2011) details the assignment of the 15 CLM4 PFTs using the Hurtt et al. (2006) data types during 1850–2005.

2.3 Mapping atmospheric CO_2 from surface fluxes

Although the CESM simulated the three-dimensional structure of atmospheric CO_2, we used a pulse-response transport operator to separate the imprints of CO_2 fluxes from different regions on the hemispheric CO_2 patterns. The transport operator was developed using the GEOS-Chem transport model (version 9.1.2, Nassar et al. (2010)). GEOS-Chem was configured as in Keppel-Aleks et al. (2013) on a $4^\circ \times 5^\circ$ horizontal grid with 47 vertical layers, and forced with meteorology fields from the 3–6-hourly Modern Era Retrospective-Analysis for Research and Applications (MERRA) reanalysis dataset (Rienecker et al., 2011). A tagged 1 Pg C month^{-1} pulse was released for each of the 20 terrestrial source regions in Fig. 1 for each calendar month. Each 1 Pg C month^{-1} pulse was distributed spatially according to monthly fluxes from the Carnegie-Ames-Stanford Approach (CASA) fluxes from Olsen and Randerson (2004). Following the year in which pulses were released, the signals were allowed to decay for 60 subsequent months until CO_2 was well-mixed in the atmosphere. We then sampled GEOS-Chem at the locations of 41 NOAA cooperative CO_2 flask sample sites (Dlugokencky et al. (2013); Table 1, Fig. 1) for each month simulated. This resulted in a CO_2 transport operator matrix with dimensions $N_{reg.} \times N_{obs.} \times N_{mon.}$.

We aggregated NEP fluxes from CLM4 to the spatial scale of the 20 source regions (Fig. 1), and used matrix multiplication to calculate CO_2 mole fraction at the observation sites. Global CO_2 was calculated from the sum of the atmospheric CO_2 responses to pulses emitted from the shaded regions in Fig. 1. We analyzed both the CO_2 fields from global fluxes and CO_2 patterns influenced only by larger regions representing Arctic, boreal, temperate, subtropical, tropical, and Southern Hemisphere (SH) ecosystems. We calculated the CO_2 annual cycle amplitude values as the peak-to-trough differences in CO_2 summed over each component region (e.g., the CO_2 annual cycle amplitude at a given station from pulses emitted from the Arctic was calculated as the peak-to-trough difference in the sum of CO_2 from pulses emitted by the blue regions in Fig. 1). We note that our analysis focuses on surface observations of atmospheric CO_2, and does not include aircraft measurements.

The spatial and temporal patterns in the annual cycle amplitudes using the pulse-response transport operator and the fully coupled CESM configuration were broadly similar. Since the land CO_2 tracer in the CAM4 is derived from NEE, we present a comparison in which we have generated CO_2 using NEE (despite that we use NEP for subsequent analyses). The magnitudes generally differed by less than 2 ppm due to different model boundary layer schemes and atmospheric transport (Fig. 2c). We note that the largest differences were during the last century of the simulation, which we hypothesize was due to shifts in atmospheric transport in response to the dramatic climate change in the CAM4. We also assessed the validity of the assumption to model only the land contributions to trends in the mean annual cycle of CO_2 by calculating the CO_2 amplitudes in the CAM land and ocean tracers. We found that the contemporary peak-to-trough amplitude in the ocean tracer averaged across our high latitude stations was 2 ppm (in contrast to 10 ppm in the land tracer). Although both the land and ocean amplitudes grow with time, by 2300, the high latitude ocean tracer had an amplitude of 3 ppm, only 18% of the land amplitude for this time period.

Biogeosciences Discuss., doi:10.5194/bg-2016-112, 2016
Manuscript under review for journal Biogeosciences
Published: 5 April 2016

Ocean carbon uptake was found to change significantly in CESM through 2300 (Randerson et al., 2015), but based on these numbers, ocean CO_2 still had a smaller imprint on the atmospheric annual cycle.

2.4 Atmospheric CO_2 timeseries analysis

We quantified observed and simulated CO_2 annual cycle amplitude at NOAA observatories before aggregating amplitudes across four latitude bands spanning 60°–90°N (NH high latitudes), 40°–60°N (NH midlatitudes), 20°–40°N (NH subtropics), and 0°–20°N (NH tropics). We identified a subset of stations in the NOAA Global Monitoring Division (Conway et al., 1994) and Scripps Institute of Oceanography (Keeling et al., 2005) networks with better than 95% temporal coverage of monthly mean values from 1985–2013 (gray circles in Fig. 1). The trends at these stations were calculated iteratively as a second-order polynomial, as described by Keppel-Aleks et al. (2013). After subtracting the trend from the raw observations, we calculated the peak-to-trough amplitude (A^{Obs}) for each calendar year in which observations existed. We then aggregated A^{obs} from all stations within the specified latitude bands to determine a regionally averaged amplitude.

We calculated the regional CO_2 amplitudes for the fully coupled simulations (A^{FC}) using a nearly identical methodology. However, due to the length of the simulated timeseries, we detrended the data in ten-year increments. For CESM output, we used only the sampling locations with greater than 95% temporal coverage for comparison with the observations (Fig. 1, gray circles), but aggregated amplitudes at a larger set of marine boundary layer observatories when assessing future trends (Fig. 1, black circles). Due to the flexible transport operator, we separately calculated amplitudes from NoRad (A^{NoRad}), and NoLUC (A^{NoLUC}) simulations, and were further able to simulate only the contribution from specified ecosystem types. The contribution of climate change to the CO_2 mean annual cycle amplitude (A^{Clim}) was calculated from the difference between A^{FC} and A^{NoRad}. Likewise, the LUC contribution to the annual cycle amplitude was calculated from the difference between A^{FC} and A^{NoLuc}.

3 Results

3.1 Trends in present-day observed and modeled CO_2 annual cycle amplitudes

Throughout the NH, the CESM simulated both smaller mean annual cycle amplitudes and a smaller trends in amplitude relative to observations. The CESM underestimated the magnitudes of A^{Obs} by roughly 50% (Fig. 3b, c). The 1985–2013 mean A^{Obs} averaged over the whole NH was 9.5 ppm, while A^{FC} was 5.9 ppm. At high latitudes, the observed value was 16.0 ppm, but only 10.1 ppm in the CESM, broadly consistent with Keppel-Aleks et al. (2013) who showed that the CESM1(BGC) underestimated NH seasonality by 25–40%. The CESM simulated a 17% relative increase the NH mean amplitude between 1985 and 2013 that was close to the observed 20% increase during this period. We note that the environmental drivers of amplitude increase during 1985–2013 were also simulated reasonably well by CESM: the annual mean NH atmospheric CO_2 mole fraction in CESM was 425 ppm compared to observations of 391 ppm in 2010, and the NH atmospheric temperature increase over land was also roughly equivalent (1.02 K vs 0.95 K in the NCEP-NCAR Reanalysis (Kalnay et al., 1996)).

Biogeosciences Discuss., doi:10.5194/bg-2016-112, 2016
Manuscript under review for journal Biogeosciences
Published: 5 April 2016

Consistent with the observations, the CESM simulated an increasing amplitude trend with latitude over the NH. However, the meridional gradient in the CESM was too weak, resulting in much smaller trends over the high latitudes. The modeled trend in the CO_2 annual cycle amplitude over the high latitudes was 0.05 ppm yr^{-1} (0.46% yr^{-1}) for the 1985–2013 period, while the observed trend was 0.09 ppm yr^{-1} (0.57% yr^{-1}). Midlatitude and subtropical trends simulated by the CESM were around 0.03 ppm yr^{-1} (0.40% yr^{-1} and 0.47% yr^{-1}, respectively), and the trends in the magnitudes were closer to the observed midlatitude trend of 0.04 ppm yr^{-1} (0.22% yr^{-1}) and subtropical trend of 0.05 ppm yr^{-1} (0.61% yr^{-1}).

3.2 Future CO_2 annual cycle amplitude changes

3.2.1 Total amplitude changes

Both bottom-level atmospheric temperature and the mean atmospheric CO_2 mole fraction increased markedly in CESM through 2300. Due to the imposed emission scenario, the rate of atmospheric CO_2 mole fraction increase rose from about 1.7 ppm yr^{-1} during 1950–2000 to 11.0 ppm yr^{-1} between 2050 and 2150, then declined to approximately 0.5 ppm yr^{-1} during the final 50 years of the simulation. The mean atmospheric CO_2 mole fraction in the FullyCoupled simulation increased by over 800 ppm by 2100 and by over 2000 ppm by 2300 (Fig. 4a). In the NoRad simulation, where CO_2 did not exert a radiative forcing, the atmospheric mole fraction followed a similar pattern of increase, but equilibrated at a lower mean value by 2200. We note that the atmospheric CO_2 mole fraction values were diagnostic only, and the biogeochemical and radiative processes in the CESM responded to the lower mole fraction values prescribed according to the ECP8.5 forcing scenario indicated by the dashed black line in Fig. 4a.

In the FullyCoupled simulation, the increases in CO_2 and other radiative forcing agents resulted in a 6 K T increase by 2100 and an 11 K T increase by 2300 relative to the 1950–1959 mean (Fig. 4b). T in the NoRad simulation only increased by $\sim$2 K through 2300, which can be traced to changes in albedo and surface energy balance. For small temperature changes and high levels of CO_2 fertilization, the NoRad experiment was able to maintain a steady carbon sink between 50–60 Pg C yr^{-1} between 2100 and 2300 (Fig. 4c). In contrast, the sink in the FullyCoupled simulation reached a maximum of 56 Pg C yr^{-1} by 2120, then declined to 35–50 Pg C yr^{-1} in the last 100 years of the simulation, suggesting that the large climate change in this simulation reduced the efficiency of the global terrestrial sink with time. LUC partly offset the weakening of the land carbon sink due to climate change, increasing net terrestrial carbon uptake by up to 30 Pg C yr^{-1} after 2100.

The NH mean CO_2 annual cycle amplified by 3.1 ppm (57%) by 2100, and 4.1 ppm (76%) by 2300 from the 1950–1959 baseline in the FullyCoupled simulation (Table 4). Consistent with the observed present-day CO_2 amplification, the magnitudes of the A^{FC} increases strengthened moving poleward (Fig. 5). A^{FC} increases between 1950 and 2300 ranged from 1.4 ppm (52%) over the NH tropics to 9.2 ppm (110%) over the high latitudes. Peak A^{FC} magnitudes occurred between 2180 and 2250 (Table 3), and ranged from 4.4 ppm over the NH tropics to 17.7 ppm over the high latitudes.

Given weak seasonal exchange in the CESM, simulated CO_2 annual cycle amplitudes did not approach the contemporary mean observed mean A^{Obs} (2009–2013) until 2240 in the NH high latitudes, 2110 in the midlatitudes, and 2100 in the subtropics (Fig. 5a, black filled squares). Over the NH tropics, peak A^{FC} occurred by 2240, but was still 0.6 ppm below current A^{Obs}.

Biogeosciences Discuss., doi:10.5194/bg-2016-112, 2016
Manuscript under review for journal Biogeosciences
Published: 5 April 2016

The discrepancy between tropical CO_2 seasonality inferred from simulated NEP and observations reflects the non-trivial contributions of ocean and fossil fuel fluxes to the CO_2 annual cycle (Randerson et al., 1997, Table 4) and (Lindsay et al., 2014, Fig. 15). When high latitude CO_2 amplitudes reached peak values, climate change and non-radiative forcing from CO_2 fertilization and N-deposition each contributed about half of the 9.4 ppm increase (relative to the 1950–1959 baseline). At this point, Arctic temperatures were 13 K higher than the present-day baseline, midlatitude temperatures were 9 K higher (Fig. 5b, c), and the mean NH atmospheric CO_2 mole fraction was approximately 2330 ppm (Fig. 4a).

3.3 Contributions of changing atmospheric composition, climate change, and LUC to amplitude trends

3.3.1 Changing atmospheric composition effects

Changes in atmospheric composition contributed the most to CO_2 annual cycle amplification through 2300 over much of the NH (Fig. 6), with fertilization from increasing CO_2 and N-deposition adding 4 ppm to the 4.1 ppm increase in NH A^{FC} (ΔA^{FC}) between 1950 and the end of the 23rd century (Table 4). In contrast, LUC tended to reduce atmospheric CO_2 seasonality. The non-radiative component of the amplitude increase originated mainly from NH temperate regions (Fig. 7a), which accounted for 2.3 ppm of ΔA^{NoRad} at the end of the 23rd century. NH boreal regions (Fig. 8a) made the second greatest contribution to NH ΔA^{NoRad} (35%, 1.4 ppm; Table 4). The remaining 7.5% (0.4 ppm) of the NH ΔA^{NoRad} increase came from the Arctic (Fig. 9a) or subtropical/tropical ecosystems.

Temperate ecosystems had the largest response to CO_2 fertilization and N-deposition. Consistent with this large temperate response, the increase in A^{FC} from non-radiative forcing was largest over the NH midlatitudes. The effects of changing atmospheric composition in boreal ecosystems contributed another 26% to the high latitude CO_2 amplitude, 28% to the midlatitude, and 43% to the subtropical A^{FC}. Arctic CO_2 fertilization and N-deposition effects were small, consistent with CO_2 fertilization effects being proportional to gross primary production (Schimel et al., 2015). Fig. 10 shows that non-radiative forcing from boreal and temperate regions together constituted at least 40% of the increase in high latitude, midlatitude, and subtropical A^{FC} from the beginning of the 21st century through the end of the 23rd century. Furthermore, temperate CO_2 fertilization and N-deposition were the primary drivers of midlatitude CO_2 annual cycle amplification in all periods, and subtropical amplification from 2050 onward.

Our results are consistent with Randerson et al. (2015), who found that enhanced terrestrial productivity from CO_2 fertilization, as well as warming-driven increases in heterotrophic respiration (HR), over boreal and temperate regions were responsible for most of the amplification of the NH CO_2 annual cycle after 2100. The strong fertilization effect on the amplification of the NH CO_2 annual cycle is surprising given that nitrogen limitation in the CLM4 produced weaker fertilization in the CESM compared to other CMIP5 models (Thornton and Zimmermann, 2007; Piao et al., 2013; Peng and Dan, 2015).

3.3.2 Climate change effects

Climate change caused the CO_2 annual cycle amplitude to increase during the early part of the simulation, but the effect reversed in the 23rd century when the mean bottom-level atmospheric temperature had risen by 6–13 K across NH land

Biogeosciences Discuss., doi:10.5194/bg-2016-112, 2016
Manuscript under review for journal Biogeosciences
Published: 5 April 2016

regions. During the early part of the simulation, boreal (Fig. 8b) and Arctic (Fig. 9b) climate change drove the increase in NH A^{Clim}, outpacing boreal and temperate CO_2 fertilization and N-deposition effects. The increase in NH A^{Clim} largely reflected high latitude climate change effects that increased growing season temperature, leading to larger peak GPP values and a longer growing season.

By 2100, Arctic and boreal climate change increased high latitude A^{FC} by about 1 and 2 ppm (37%) from the 1950–1959 mean, respectively, outweighing the combined contributions of boreal and temperate non-radiative forcing (2.3 ppm, 26%) (Fig. 10a). After 2100, Arctic climate change had a greater effect on extratropical A^{FC} than boreal or temperate climate change, adding 1.9 ppm (23%) to high latitude, 0.7 ppm (8%) to midlatitude, and 0.45 ppm (7.6%) to the subtropical base period A^{FC} by the end of the 23rd century (Fig. 10) when temperatures surpassed 278, 288, and 298 K, respectively. Overall, the effects of temperate and boreal CO_2 fertilization and N-deposition outweighed climate change effects on CO_2 annual cycle amplification at the end of the simulation, adding 4.7 ppm (57%) to high latitude, 6.8 ppm (78%) to midlatitude, and 3.8 ppm (64%) to the subtropical base period A^{FC}.

It is worth noting that temperate climate change exerted its greatest impact on NH high latitude CO_2 before 2000 (T around 265 K), and on midlatitude and subtropical A^{FC} after 2200 (T $>$ 289 K and 299 K, respectively). After 2100, climate change reduced the seasonality of CO_2 exchange in temperate ecosystem CO_2. Climate change effects from lower latitudes made up most of the midlatitude residual after 2000, and were largest between 2100 and 2150. Low latitude climate change also made up most of the high latitude residual after 2000.

3.3.3 LUC effects

Land use change in the CESM decreased the seasonality of terrestrial CO_2 exchange and led to negative trends in the mean annual cycle amplitude. LUC reduced the hemisphere-average amplitude by 0.9 ppm (17%) in 2300 (Fig. 6c, Table 4), opposing the non-radiative forcing and climate change effects on the mean CO_2 annual cycle amplitude. The largest reductions in ΔA^{FC} due to LUC (ΔA^{LUC}) occurred over the mid- (1.3 ppm) and high latitudes (1.6 ppm), with nearly all of the negative ΔA^{LUC} effects originating from boreal (Fig. 8c) and temperate (Fig. 7c) regions. While the magnitudes of boreal and temperate LUC forcing increased from the 21st through the 23rd century over the NH extratropics (Fig. 10), the percent contribution of LUC to ΔA^{LUC} declined over time since LUC fluxes were held constant after 2100.

This finding contrasts recent results suggesting that agriculture intensification contributes significantly to positive trends in the mean annual cycle amplitude (Gray et al., 2014; Zeng et al., 2014), and likely reflects the fact that croplands were treated as unmanaged grasslands in the CESM. We note that future LUC and its effect on the seasonality of the terrestrial carbon flux depends on the integration of climate and societal impacts across several climate scenarios.

3.3.4 Changes in growing season length

The NH CO_2 annual cycle amplitude increase resulted not only from changes in the mean temperature, but also from lengthening of the growing season. We found that the growing season, defined as months with negative NEP (net terrestrial carbon uptake), increased for all NH terrestrial regions by about 1 month. The overall lengthened growing seasons accounted for

Biogeosciences Discuss., doi:10.5194/bg-2016-112, 2016
Manuscript under review for journal Biogeosciences
Published: 5 April 2016

1–1.3% yr^{-1} of the high latitude net terrestrial carbon uptake after 2050, and up to 5% yr^{-1} of the midlatitude terrestrial carbon uptake after 2100. In boreal and temperate ecosystems, this change was not evident until after 2100 (Fig. 11a). Climate change was the primary contributor in boreal and Arctic regions (Fig. 11c). In the subtropics, however, CO_2 fertilization and N-deposition lengthened the growing season (Fig. 11b), while climate change had the opposite effect. This result suggests that subtropical ecosystems in CESM are near a temperature optimum, but are water-limited. Therefore, increases in water use efficiency associated with increased atmospheric CO_2 permit longer periods of carbon uptake.

4 Discussion and Conclusions

The mean annual cycle of atmospheric CO_2 is a first order diagnostic of terrestrial carbon exchange and its trend with time integrates a range of environmental and human factors (Randerson et al., 1997). An active area of carbon cycle research is determining the extent to which coupled ESMs provide predictive skill for future carbon-climate feedbacks. We note that many of the methods used to evaluate the carbon cycle in ESMs rely on benchmarking short term responses to either seasonal or interannual climate variability (Keppel-Aleks et al., 2013) or on extrapolating future behavior based on some mechanistic link between short term and long term variability (Cox et al., 2013; Hoffman et al., 2014). The changing CO_2 annual cycle provides a unique opportunity to gauge a model's sensitivity to slow-varying climate and environmental changes, since we have observed large trends in this quantity over the instrumental record (Graven et al., 2013).

Extended Concentration Pathway simulations run in CESM with coupled biogeochemistry show that the NH mean annual cycle of atmospheric CO_2 increased by 17% from 1985 to 2013. The relative increase was in line with the observed 20% increase over the NH during the same time period. However, the spatial pattern of the percent amplitude change was more uniform throughout the NH (around 0.40–0.50% yr^{-1} across latitude bands), whereas observed relative increases ranged from 0.22% yr^{-1} in the midlatitudes to 0.57% yr^{-1} in the high latitudes. Furthermore, the trend in the magnitude of the amplitude at high latitudes was about half of the observed trend (0.05 ppm yr^{-1} vs 0.09 ppm yr^{-1}). The largest driver of the midlatitude CO_2 annual cycle amplitude trend in the CESM was temperate non-radiative forcing from CO_2 fertilization and nitrogen deposition, perhaps indicating that the model CO_2 fertilization effect was too strong.

Our analysis focused on natural drivers of the mean annual cycle, including climate change, CO_2 fertilization, and nitrogen deposition, since CESM1(BGC) did not include agricultural intensification, and land management that has been suggested as one driver of the amplitude increase over the last 50 years (Gray et al., 2014; Zeng et al., 2014). Zeng et al. (2014) suggests that up to 45% of the observed trend may be due to land use practices, with the remainder partitioned roughly equally between climate and fertilization effects. In contrast, land use change in the CESM reduced the atmospheric CO_2 annual cycle amplitude throughout the NH, with the largest reductions over the mid- and high latitudes. Decreased amplitudes possibly result from the exclusion of the effects of cropland intensification in the CESM simulations. After accounting for land management contributions to the amplitude increase, the sensitivity of the CO_2 amplitude to natural factors may be reasonable. Our results suggest that model development focused on human modification of carbon fluxes (e.g., by agriculture (Levis et al., 2014) or by disturbance (Kloster et al., 2012)) may facilitate improved comparison both of mean behavior and trends.

Biogeosciences Discuss., doi:10.5194/bg-2016-112, 2016
Manuscript under review for journal Biogeosciences
Published: 5 April 2016

We note, however, that CESM1(BGC) does have overall biases in seasonality. Low seasonality, together with low absolute rates of increase, meant that the CESM mean annual cycle did not approach present values over the NH extratropics until the 22nd century. CESM1(BGC) did not include paramaterizations for permafrost carbon dynamics, which have since been improved in CESM (Koven et al., 2015). Thus, short soil carbon turnover time in CLM4 may have contributed to the amplitude underestimation by damping ecosystem respiration outside of the growing season (Keppel-Aleks et al., 2013; Koven et al., 2013) and would affect both baseline values and trends. In addition, Forkel et al. (2016) found that interaction between climate change and changes in vegetation cover over northern high latitudes was the primary driver of the north-south gradient in observed NH atmospheric CO_2 seasonal amplitude trends, indicating that the lack of dynamic vegetation in the CLM4 likely contributes to underestimation of the seasonal amplitudes by the CESM.

Additionally, we found that the net land sink began to decrease prior to amplitude decreasing. Until 2100, NEP became more negative (sink strength increased) while the mean annual cycle amplitude also increased. After 2100, the magnitude of NEP decreased (sink strength decreased), likely reflecting enhanced subtropical respiration, while the amplitude continued to increase until after 2250 as a result of increased productivity due to longer growing seasons. This underscores that while increasing amplitude may reflect enhanced seasonality of uptake, it does not necessitate enhanced annually integrated uptake.

By running CESM to 2300 with the ECP boundary conditions, we were able to simulate notable carbon cycle interactions that were not apparent before 2100, the nominal end date for CMIP5 runs. We found that the mean NH atmospheric CO_2 annual cycle amplitude increased by 57% from 1950 to 2100, and by an additional 20% by 2300 in the CESM1(BGC). These rates of increase resulted primarily from CO_2 fertilization and nitrogen deposition in temperate and boreal ecosystems. Initially, climate change in boreal and Arctic ecosystems also contributed to NH amplitude increases (over half the amplification prior to 2100), but increases in respiration relative to GPP at lower latitudes meant that by the 23rd century, climate change no longer led to increasing amplitude. These results indicate that there is no high-temperature tipping point at which terrestrial productivity declines in the CESM.

Acknowledgements. This research was supported in part by the Biogeochemistry – Climate Feedbacks Scientific Focus Area (SFA), which is sponsored by the Regional and Global Climate Modeling (RGCM) Program in the Climate and Environmental Sciences Division (CESD) of the Biological and Environmental Research Program in the U.S. Department of Energy Office of Science.

The National Center for Atmospheric Research (NCAR) is sponsored by the National Science Foundation.

Computing resources were provided by the Climate Simulation Laboratory at NCAR's Computational and Information Systems Laboratory (CISL), sponsored by the National Science Foundation and other agencies.

We gratefully acknowledge Ernesto Munoz for running and processing the CESM simulations.

Biogeosciences Discuss., doi:10.5194/bg-2016-112, 2016
Manuscript under review for journal Biogeosciences
Published: 5 April 2016

References

Angert, A., Biraud, S., Bonfils, C., Henning, C. C., Buermann, W., Pinzon, J., Tucker, C. J., and Fung, I.: Drier summers cancel out the CO_2 uptake enhancement induced by warmer springs, P. Natl. Acad. Sci., 102, 10 823–10 827, http://www.pnas.org/content/102/31/10823, 2005.

Bacastow, R. B., Keeling, C. D., and Whorf, T. P.: Seasonal amplitude increase in atmospheric CO_2 concentration at Mauna Loa, Hawaii, 1959–1982, J. Geophys. Res. Atmos., 90, 10 529–10 540, doi:10.1029/JD090iD06p10529, http://dx.doi.org/10.1029/JD090iD06p10529, 1985.

Barichivich, J., Briffa, K. R., Myneni, R. B., Osborn, T. J., Melvin, T. M., Ciais, P., Piao, S., and Tucker, C.: Large-scale variations in the vegetation growing season and annual cycle of atmospheric CO_2 at high northern latitudes from 1950 to 2011, Glob. Change Biol., 19, 3167–3183, doi:10.1111/gcb.12283, http://dx.doi.org/10.1111/gcb.12283, 2013.

Buermann, W., Bikash, P. R., Jung, M., Burn, D. H., and Reichstein, M.: Earlier springs decrease peak summer productivity in North American boreal forests, Env. Res. Lett., 8, 024 027, doi:10.1088/1748-9326/8/2/024027, 2013.

Claussen, M., Mysak, L., Weaver, A., Crucifix, M., Fichefet, T., Loutre, M.-F., Weber, S., Alcamo, J., Alexeev, V., Berger, A., Calov, R., Ganopolski, A., Goosse, H., Lohmann, G., Lunkeit, F., Mokhov, I., Petoukhov, V., Stone, P., and Wang, Z.: Earth system models of intermediate complexity: closing the gap in the spectrum of climate system models, Clim. Dynam., 18, 579–586, doi:10.1007/s00382-001-0200-1, http://dx.doi.org/10.1007/s00382-001-0200-1, 2002.

Cleveland, W. S., Freeny, A. E., and Graedel, T. E.: The seasonal component of atmospheric CO_2: Information from new approaches to the decomposition of seasonal time series, J. Geophys. Res. Oceans, 88, 10 934–10 946, doi:10.1029/JC088iC15p10934, http://dx.doi.org/10.1029/JC088iC15p10934, 1983.

Conway, T. J., Tans, P. P., Waterman, L. S., Thoning, K. W., Kitzis, D. R., Masarie, K. A., and Zhang, N.: Evidence for interannual variability of the carbon cycle from the National Oceanic and Atmospheric Administration/Climate Monitoring and Diagnostics Laboratory global air sampling network, J. Geophys. Res. Atmos., 99, 22 831–22 855, 1994.

Cox, P. M., Pearson, D., Booth, B. B., Friedlingstein, P., Huntingford, C., Jones, C. D., and Luke, C. M.: Sensitivity of tropical carbon to climate change constrained by carbon dioxide variability, Nature, 494, 341–344, doi:10.1038/nature11882, http://dx.doi.org/10.1038/nature11882, 2013.

Dettinger, M. D. and Ghil, M.: Seasonal and interannual variations of atmospheric CO_2 and climate, Tellus B, 50, 1–24, 1998.

Dlugokencky, E. J., Lang, P. M., Masarie, K., Crotwell, A. M., and Crotwell, M. J.: Atmospheric carbon dioxide dry air mole fractions from the NOAA ESRL carbon cycle cooperative global air sampling network, 1968–2012, 2013.

Enting, I. G. and Mansbridge, J. V.: Seasonal sources and sinks of atmospheric CO_2 Direct inversion of filtered data, Tellus B, 41B, 111–126, doi:10.1111/j.1600-0889.1989.tb00129.x, http://dx.doi.org/10.1111/j.1600-0889.1989.tb00129.x, 1989.

Forkel, M., Carvalhais, N., Rödenbeck, C., Keeling, R., Heimann, M., Thonicke, K., Zaehle, S., and Reichstein, M.: Enhanced seasonal CO_2 exchange caused by amplified plant productivity in northern ecosystems, Science, doi:10.1126/science.aac4971, http://science.sciencemag.org/content/early/2016/01/20/science.aac4971, 2016.

Graven, H. D., Keeling, R. F., Piper, S. C., Patra, P. K., Stephens, B. B., Wofsy, S. C., Welp, L. R., Sweeney, C., Tans, P. P., Kelley, J. J., Daube, B. C., Kort, E. A., Santoni, G. W., and Bent, J. D.: Enhanced Seasonal Exchange of CO_2 by Northern Ecosystems Since 1960, Science, 341, 1085–1089, doi:10.1126/science.1239207, http://www.sciencemag.org/content/341/6150/1085.abstract, 2013.

Biogeosciences Discuss., doi:10.5194/bg-2016-112, 2016
Manuscript under review for journal Biogeosciences
Published: 5 April 2016

Gray, J. M., Frolking, S., Kort, E. A., Ray, D. K., Kucharik, C. J., Ramankutty, N., and Friedl, M. A.: Direct human influence on atmospheric CO_2 seasonality from increased cropland productivity, Nature, 515, 398–401, doi:10.1038/nature13957, http://dx.doi.org/10.1038/nature13957, 2014.

Hoffman, F. M., Randerson, J. T., Arora, V. K., Bao, Q., Cadule, P., Ji, D., Jones, C. D., Kawamiya, M., Khatiwala, S., Lindsay, K., Obata, A., Shevliakova, E., Six, K. D., Tjiputra, J. F., Volodin, E. M., and Wu, T.: Causes and implications of persistent atmospheric carbon dioxide biases in Earth System Models, J. Geophys. Res. Biogeosci., 119, 141–162, doi:10.1002/2013JG002381, http://dx.doi.org/10.1002/2013JG002381, 2014.

Hurrell, J. W., Holland, M. M., Gent, P. R., Ghan, S., Kay, J. E., Kushner, P. J., Lamarque, J.-F., Large, W. G., Lawrence, D., Lindsay, K., Lipscomb, W. H., Long, M. C., Mahowald, N., Marsh, D. R., Neale, R. B., Rasch, P., Vavrus, S., Vertenstein, M., Bader, D., Collins, W. D., Hack, J. J., Kiehl, J., and Marshall, S.: The Community Earth System Model: A Framework for Collaborative Research, Bull. Amer. Meteor. Soc., 94, 1339–1360, doi:10.1175/BAMS-D-12-00121.1, http://dx.doi.org/10.1175/BAMS-D-12-00121.1, 2013.

Hurtt, G. C., Frolking, S., Fearon, M. G., Moore, B., B., Shevliakova, E., E., Malyshev, S., Pacala, S. W., and Houghton, R. A.: The underpinnings of land-use history: three centuries of global gridded land-use transitions, wood-harvest activity, and resulting secondary lands, Glob. Change Biol., 12, 1208–1229, doi:10.1111/j.1365-2486.2006.01150.x, http://dx.doi.org/10.1111/j.1365-2486.2006.01150.x, 2006.

Kalnay, E., Kanamitsu, M., Kistler, R., Collins, W., D.Deaven, Gandin, L., Iredell, M., Saha, S., White, G., Woollen, J., Zhu, Y., Chelliah, M., Ebisuzaki, W., Higgins, W., Janowiak, J., Mo, K. C., Ropelewski, C., Wang, J., , Leetma, A., Reynolds, R., Jenne, R., and Joseph, D.: The NCEP/NCAR 40-year reanalysis project, Bull. Amer. Meteor. Soc., 77, 437–470, 1996.

Keeling, C. D., Chin, J. F. S., and Whorf, T. P.: Increased activity of northern vegetation inferred from atmospheric CO_2 measurements, Nature, 382, 146–149, doi:10.1038/382146a0, http://dx.doi.org/10.1038/382146a0, 1996.

Keeling, C. D., Piper, S. C., Bacastow, R. B., Wahlen, M., Whorf, T. P., Heimann, M., and Meijer, H. A.: Atmospheric CO_2 and $13CO_2$ Exchange with the Terrestrial Biosphere and Oceans from 1978 to 2000: Observations and Carbon Cycle Implications, in: Ecological Studies, edited by Baldwin, I. T., Caldwell, M. M., Heldmaier, G., Jackson, R. B., Lange, O. L., Mooney, H., Schulze, E. D., Sommer, U., Ehleringer, J. R., M., D. D., and Cerling, T. E., vol. 177, pp. 83–113, Springer New York, doi:10.1007/0-387-27048-5_5, http://dx.doi.org/10.1007/0-387-27048-5_5, 2005.

Keenan, T. F., Hollinger, D. Y., Bohrer, G., Dragoni, D., Munger, J. W., Schmid, H. P., and Richardson, A. D.: Increase in forest water-use efficiency as atmospheric carbon dioxide concentrations rise, Nature, 499, 324–327, doi:10.1038/nature12291, http://dx.doi.org/10.1038/nature12291, 2013.

Keppel-Aleks, G., Randerson, J. T., Lindsay, K., Stephens, B. B., Moore, J. K., Doney, S. C., Thornton, P. E., Mahowald, N. M., Hoffman, F. M., Sweeney, C., et al.: Atmospheric carbon dioxide variability in the Community Earth System Model: Evaluation and transient dynamics during the 20th and 21st centuries, J. Climate, 26, 4447–4475, doi:10.1175/JCLI-D-12-00589.1, 2013.

Kloster, S., Mahowald, N. M., Randerson, J. T., and Lawrence, P. J.: The impacts of climate, land use, and demography on fires during the 21st century simulated by CLM-CN, Biogeosciences, 9, 509–525, doi:10.5194/bg-9-509-2012, http://www.biogeosciences.net/9/509/2012/, 2012.

Kohlmaier, G. H., Siré, E.-O., Janecek, A., Keeling, C. D., Piper, S. C., and Revelle, R.: Modelling the seasonal contribution of a CO_2 fertilization effect of the terrestrial vegetation to the amplitude increase in atmospheric CO_2 at Mauna Loa Observatory, Tellus B, 41B, 487–510, doi:10.1111/j.1600-0889.1989.tb00137.x, http://dx.doi.org/10.1111/j.1600-0889.1989.tb00137.x, 1989.

Komhyr, W. D., Gammon, R. H., Harris, T. B., Waterman, L. S., Conway, T. J., Taylor, W. R., and Thoning, K. W.: Global atmospheric CO_2 distribution and variations from 1968–1982 NOAA/GMCC CO_2 flask sample data, J. Geophys. Res. Atmos., 90, 5567–5596, doi:10.1029/JD090iD03p05567, http://dx.doi.org/10.1029/JD090iD03p05567, 1985.

Koven, C. D., Riley, W. J., Subin, Z. M., Tang, J. Y., Torn, M. S., Collins, W. D., Bonan, G. B., Lawrence, D. M., and Swenson, S. C.: The effect of vertically resolved soil biogeochemistry and alternate soil C and N models on C dynamics of CLM4, Biogeosciences, 10, 7109–7131, doi:10.5194/bg-10-7109-2013, http://www.biogeosciences.net/10/7109/2013/, 2013.

Koven, C. D., Lawrence, D. M., and Riley, W. J.: Permafrost carbon-climate feedback is sensitive to deep soil carbon decomposability but not deep soil nitrogen dynamics, P. Natl. Acad. of Sci., doi:10.1073/pnas.1415123112, 2015.

Lamarque, J.-F., Bond, T. C., Eyring, V., Granier, C., Heil, A., Klimont, Z., Lee, D., Liousse, C., Mieville, A., Owen, B., Schultz, M. G., Shindell, D., Smith, S. J., Stehfest, E., Van Aardenne, J., Cooper, O. R., Kainuma, M., Mahowald, N., McConnell, J. R., Naik, V., Riahi, K., and van Vuuren, D. P.: Historical (1850–2000) gridded anthropogenic and biomass burning emissions of reactive gases and aerosols: methodology and application, Atmos. Chem. Phys., 10, 7017–7039, doi:10.5194/acp-10-7017-2010, http://www.atmos-chem-phys.net/10/7017/2010/, 2010.

Lawrence, D. M., Oleson, K. W., Flanner, M. G., Thornton, P. E., Swenson, S. C., Lawrence, P. J., Zeng, X., Yang, Z.-L., Levis, S., Sakaguchi, K., Bonan, G. B., and Slater, A. G.: Parameterization improvements and functional and structural advances in Version 4 of the Community Land Model, J. Adv. Model. Earth Syst., 3, M03 001, doi:10.1029/2011MS000045, http://dx.doi.org/10.1029/2011MS000045, 2011.

Lawrence, D. M., Oleson, K. W., Flanner, M. G., Fletcher, C. G., Lawrence, P. J., Levis, S., Swenson, S. C., and Bonan, G. B.: The CCSM4 land simulation, 1850-2005: Assessment of surface climate and new capabilities, J. Climate, doi:10.1175/JCLI-D-11-00103.1, 2012.

Levis, S., Hartman, M. D., and Bonan, G. B.: The Community Land Model underestimates land-use CO_2 emissions by neglecting soil disturbance from cultivation, Geoscientific Model Development, 7, 613–620, doi:10.5194/gmd-7-613-2014, http://www.geosci-model-dev.net/7/613/2014/, 2014.

Lindsay, K., Bonan, G. B., Doney, S. C., Hoffman, F. M., Lawrence, D. M., Long, M. C., Mahowald, N. M., Keith Moore, J., Randerson, J. T., and Thornton, P. E.: Preindustrial-Control and Twentieth-Century Carbon Cycle Experiments with the Earth System Model CESM1(BGC), J. Climate, 27, 8981–9005, doi:10.1175/JCLI-D-12-00565.1, http://dx.doi.org/10.1175/JCLI-D-12-00565.1, 2014.

Liu, M., Wu, J., Zhu, X., He, H., Jia, W., and Xiang, W.: Evolution and variation of atmospheric carbon dioxide concentration over terrestrial ecosystems as derived from eddy covariance measurements, Atmospheric Environment, 114, 75–82, http://www.sciencedirect.com/science/article/pii/S1352231015300996, 2015.

Luo, Y., Su, B., Currie, W. S., Dukes, J. S., Finzi, A., Hartwig, U., Hungate, B., McMurtrie, R. E., Oren, R., Parton, W. J., Pataki, D. E., Shaw, R. M., Zak, D. R., and Field, C. B.: Progressive Nitrogen Limitation of Ecosystem Responses to Rising Atmospheric Carbon Dioxide, BioScience, 54, 731–739, doi:10.1641/0006-3568(2004)054[0731:PNLOER]2.0.CO;2, http://bioscience.oxfordjournals.org/content/54/8/731.abstract, 2004.

Manning, M. R.: Seasonal Cycles in Atmospheric CO_2 Concentrations, in: NATO ASI Series, edited by Heimann, M., vol. 15, pp. 65–94, Springer Berlin Heidelberg, http://dx.doi.org/10.1007/978-3-642-84608-3_3, 1993.

McDonald, K. C., Kimball, J. S., Njoku, E., Zimmermann, R., and Zhao, M.: Variability in Springtime Thaw in the Terrestrial High Latitudes: Monitoring a Major Control on the Biospheric Assimilation of Atmospheric CO_2 with Spaceborne Microwave Remote Sensing, Earth Interact., 8, 1–23, doi:10.1175/1087-3562(2004)8<1:VISTIT>2.0.CO;2, http://dx.doi.org/10.1175/1087-3562(2004)8<1:VISTIT>2.0.CO;2, 2004.

McGuire, A. D., Sitch, S., Clein, J. S., Dargaville, R., Esser, G., Foley, J., Heimann, M., Joos, F., Kaplan, J., Kicklighter, D. W., Meier, R. A., Melillo, J. M., Moore, B., Prentice, I. C., Ramankutty, N., Reichenau, T., Schloss, A., Tian, H., Williams, L. J., and Wittenberg, U.: Carbon balance of the terrestrial biosphere in the Twentieth Century: Analyses of CO_2, climate and land use effects with four process-based ecosystem models, Glob. Biogeochem. Cycles, 15, 183–206, doi:10.1029/2000GB001298, http://dx.doi.org/10.1029/2000GB001298, 2001.

Meinshausen, M., Smith, S., Calvin, K., Daniel, J., Kainuma, M., Lamarque, J.-F., Matsumoto, K., Montzka, S., Raper, S., Riahi, K., Thomson, A., Velders, G., and van Vuuren, D.: The RCP greenhouse gas concentrations and their extensions from 1765 to 2300, Climatic Change, 109, 213–241, doi:10.1007/s10584-011-0156-z, http://dx.doi.org/10.1007/s10584-011-0156-z, 2011.

Nassar, R., Jones, D. B. A., Suntharalingam, P., Chen, J. M., Andres, R. J., Wecht, K. J., Yantosca, R. M., Kulawik, S. S., Bowman, K. W., Worden, J. R., Machida, T., and Matsueda, H.: Modeling global atmospheric CO_2 with improved emission inventories and CO_2 production from the oxidation of other carbon species, Geoscientific Model Development, 3, 689–716, doi:10.5194/gmd-3-689-2010, http://www.geosci-model-dev.net/3/689/2010/, 2010.

Neale, R. B., Richter, J., Park, S., Lauritzen, P. H., Vavrus, S. J., Rasch, P. J., and Zhang, M.: The Mean Climate of the Community Atmosphere Model (CAM4) in forced SST and Fully Coupled Experiments, J. Climate, 26, 5150–5168, doi:10.1175/JCLI-D-12-00236.1, http://dx.doi.org/10.1175/JCLI-D-12-00236.1, 2013.

Nemry, B., Francois, L., Warnant, P., Robinet, F., and Gerard, J. C.: The seasonality of the CO_2 exchange between the atmosphere and the land biosphere: A study with a global mechanistic vegetation model, J. Geophys. Res. Atmos., 101, 7111–7125, doi:10.1029/95JD03656, http://dx.doi.org/10.1029/95JD03656, 1996.

Olsen, S. C. and Randerson, J. T.: Differences between surface and column atmospheric CO_2 and implications for carbon cycle research, J. Geophys. Res. Atmos., 109, D02 301, doi:10.1029/2003JD003968, http://dx.doi.org/10.1029/2003JD003968, 2004.

Parida, B. R. and Buermann, W.: Increasing summer drying in North American ecosystems in response to longer nonfrozen periods, Geophys. Res. Lett., 41, 5476–5483, doi:10.1002/2014GL060495, http://dx.doi.org/10.1002/2014GL060495, 2014.

Pearman, G. I. and Hyson, P.: The annual variation of atmospheric CO_2 concentration observed in the Northern Hemisphere, J. Geophys. Res, 86, 9839–9843, doi:10.1029/JC086iC10p09839, http://dx.doi.org/10.1029/JC086iC10p09839, 1981.

Peng, J. and Dan, L.: Impacts of CO_2 concentration and climate change on the terrestrial carbon flux using six global climate-carbon coupled models, Ecological Modelling, 304, 69–83, http://www.sciencedirect.com/science/article/pii/S0304380015000721, 2015.

Piao, S., Sitch, S., Ciais, P., Friedlingstein, P., Peylin, P., Wang, X., Ahlstrom, A., Anav, A., Canadell, J. G., Cong, N., Huntingford, C., Jung, M., Levis, S., Levy, P. E., Li, J., Lin, X., Lomas, M. R., Lu, M., Luo, Y., Ma, Y., Myneni, R. B., Poulter, B., Sun, Z., Wang, T., Viovy, N., Zaehle, S., and Zeng, N.: Evaluation of terrestrial carbon cycle models for their response to climate variability and to CO_2 trends, Glob. Change Biol., 19, 2117–2132, doi:10.1111/gcb.12187, http://dx.doi.org/10.1111/gcb.12187, 2013.

Prentice, I. C., Farquhar, G. D., Fasham, M. J. R., Goulden, M. L., Heimann, M., Jaramillo, V. J., Kheshgi, H. S., LeQuéré, C., Scholes, R. J., and Wallace, D. W. R.: Climate Change 2001: The Scientific Basis. Contribution of Working Group I to the Third Assessment Report of the Intergovernmental Panel on Climate Change, chap. 3: The Carbon Cycle and Atmospheric Carbon Dioxide Content, p. 881pp, Cambridge University Press, 2001.

Randerson, J. T., Thompson, M. V., Conway, T. J., Fung, I. Y., and Field, C. B.: The contribution of terrestrial sources and sinks to trends in the seasonal cycle of atmospheric carbon dioxide, Glob. Biogeochem. Cycles, 11, 535–560, doi:10.1029/97GB02268, http://dx.doi.org/10.1029/97GB02268, 1997.

Randerson, J. T., Field, C. B., Fung, I. Y., and Tans, P. P.: Increases in early season ecosystem uptake explain recent changes in the seasonal cycle of atmospheric CO_2 at high northern latitudes, Geophys. Res. Lett., 26, 2765–2768, doi:10.1029/1999GL900500, http://dx.doi.org/10.1029/1999GL900500, 1999.

Randerson, J. T., Lindsay, K., Munoz, E., Fu, W., Moore, J. K., Hoffman, F. M., Mahowald, N. M., and Doney, S. C.: Multicentury changes in ocean and land contributions to the climate-carbon feedback, Glob. Biogeochem. Cycles, 29, 744–759, doi:10.1002/2014GB005079, http://dx.doi.org/10.1002/2014GB005079, 2014GB005079, 2015.

Rienecker, M. M., Suarez, M. J., Gelaro, R., Todling, R., Bacmeister, J., Liu, E., Bosilovich, M. G., Schubert, S. D., Takacs, L., Kim, G.-K., Bloom, S., Chen, J., Collins, D., Conaty, A., da Silva, A., Gu, W., Joiner, J., Koster, R. D., Lucchesi, R., Molod, A., Owens, T., Pawson, S., Pegion, P., Redder, C. R., Reichle, R., Robertson, F. R., Ruddick, A. G., Sienkiewicz, M., and Woollen, J.: MERRA: NASAś Modern-Era Retrospective Analysis for Research and Applications, J. Climate, 24, 3624–3648, doi:10.1175/JCLI-D-11-00015.1, http://dx.doi.org/10.1175/JCLI-D-11-00015.1, 2011.

Rotty, R. M.: Estimates of seasonal variation in fossil fuel CO_2 emissions, Tellus B, 39B, 184–202, doi:10.1111/j.1600-0889.1987.tb00281.x, http://dx.doi.org/10.1111/j.1600-0889.1987.tb00281.x, 1987.

Schimel, D., Stephens, B. B., and Fisher, J. B.: Effect of increasing CO_2 on the terrestrial carbon cycle, P. Natl. Ac. Sci., doi:10.1073/pnas.1407302112, http://www.pnas.org/content/early/2014/12/25/1407302112.abstract, 2015.

Thonicke, K., Venevsky, S., Sitch, S., and Cramer, W.: The Role of Fire Disturbance for Global Vegetation Dynamics: Coupling Fire into a Dynamic Global Vegetation Model, Global Ecology and Biogeography, 10, 661–677, http://www.jstor.org/stable/3182693, 2001.

Thornton, P. E. and Zimmermann, N. E.: An Improved Canopy Integration Scheme for a Land Surface Model with Prognostic Canopy Structure, J. Climate, 20, 3902–3923, doi:10.1175/JCLI4222.1, http://dx.doi.org/10.1175/JCLI4222.1, 2007.

Thornton, P. E., Lamarque, J.-F., Rosenbloom, N. A., and Mahowald, N. M.: Influence of carbon-nitrogen cycle coupling on land model response to CO_2 fertilization and climate variability, Glob. Biogeochem. Cycles, 21, GB4018, doi:10.1029/2006GB002868, http://dx.doi.org/10.1029/2006GB002868, 2007.

Vitousek, P. M. and Howarth, R. W.: Nitrogen limitation on land and in the sea: How can it occur?, Biogeochemistry, 13, 87–115, doi:10.1007/BF00002772, http://dx.doi.org/10.1007/BF00002772, 1991.

Welp, L. R., Randerson, J. T., and Liu, H. P.: Seasonal exchange of CO_2 and $\Delta^{18}CO_2$ varies with postfire succession in boreal forest ecosystems, J. Geophys. Res. Biogeosci., 111, doi:10.1029/2005JG000126, http://dx.doi.org/10.1029/2005JG000126, 2006.

Wittenberg, U., Heimann, M., Esser, G., McGuire, A. D., and Sauf, W.: On the influence of biomass burning on the seasonal CO_2 Signal as observed at monitoring stations, Glob. Biogeochem. Cycles, 12, 531–544, doi:10.1029/98GB01532, http://dx.doi.org/10.1029/98GB01532, 1998.

Zeng, N., Zhao, F., Collatz, G. J., Kalnay, E., Salawitch, R. J., West, T. O., and Guanter, L.: Agricultural Green Revolution as a driver of increasing atmospheric CO_2 seasonal amplitude, Nature, 515, 394–397, doi:10.1038/nature13893, http://www.nature.com/nature/journal/v515/n7527/full/nature13893.html, 2014.

Zimov, S. A., Davidov, S. P., Zimova, G. M., Davidova, A. I., Chapin, F. S., Chapin, M. C., and Reynolds, J. F.: Contribution of Disturbance to Increasing Seasonal Amplitude of Atmospheric CO_2, Science, 284, 1973–1976, doi:10.1126/science.284.5422.1973, http://www.sciencemag.org/content/284/5422/1973.abstract, 1999.

Biogeosciences Discuss., doi:10.5194/bg-2016-112, 2016
Manuscript under review for journal Biogeosciences
Published: 5 April 2016

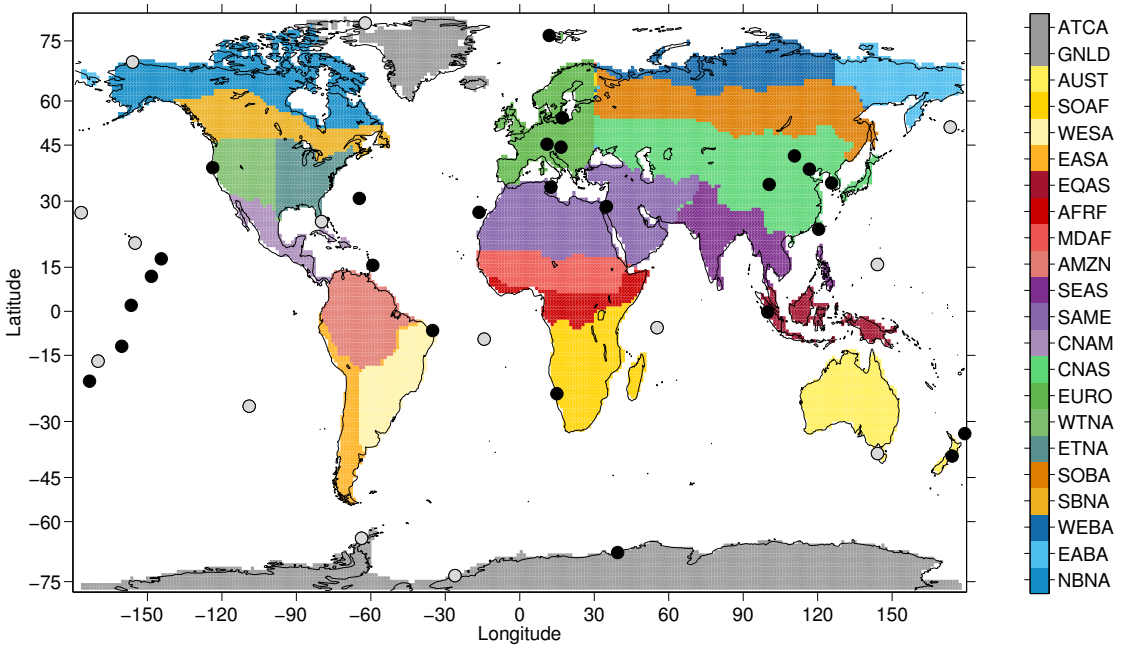

Figure 1. Map of stations where CO_2 from the pulse response code is computed. Table 1 lists the station identifiers and locations. Regions defined in the pulse response code (see Table 2) are shaded and grouped according the Arctic, NH boreal, NH temperate, NH subtropics, tropics, and SH land regions defined by Graven et al. (2013). Greenland and Antarctica were excluded from the analysis. Gray circles indicate a subset of stations from which the atmospheric annual CO_2 amplitudes were computed from 1985–2013 monthly mean observations (bold stations in Table 1).

Biogeosciences Discuss., doi:10.5194/bg-2016-112, 2016
Manuscript under review for journal Biogeosciences
Published: 5 April 2016

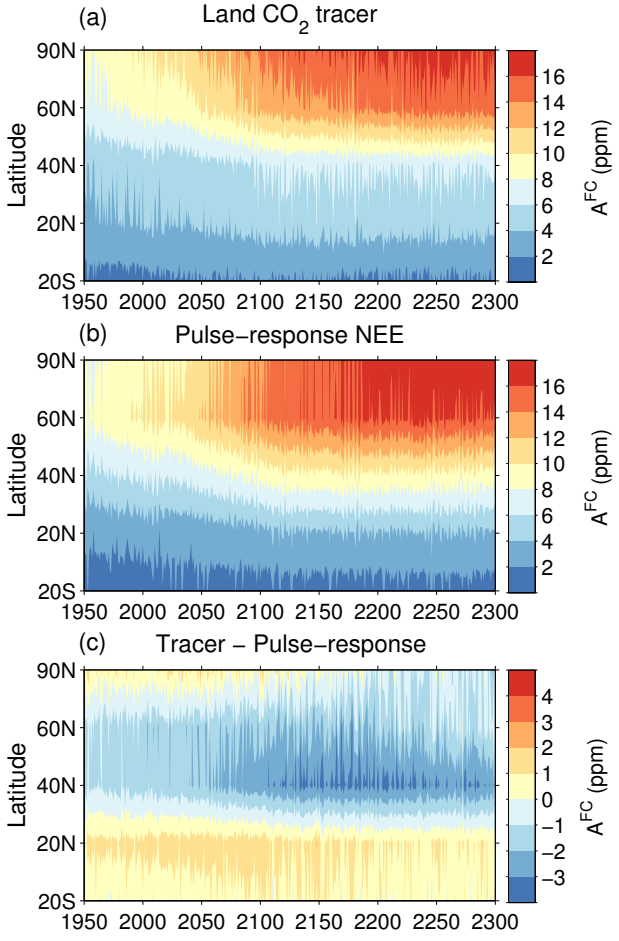

Figure 2. 10-year moving average of CO_2 annual cycle amplitudes in the FullyCoupled simulation derived from (a) the CESM land CO_2 tracer, and (b) running NEE from the CLM4 through the pulse-response code. (c) The difference between the land tracer and NEE-derived CO_2 annual cycle amplitudes.

Biogeosciences Discuss., doi:10.5194/bg-2016-112, 2016
Manuscript under review for journal Biogeosciences
Published: 5 April 2016

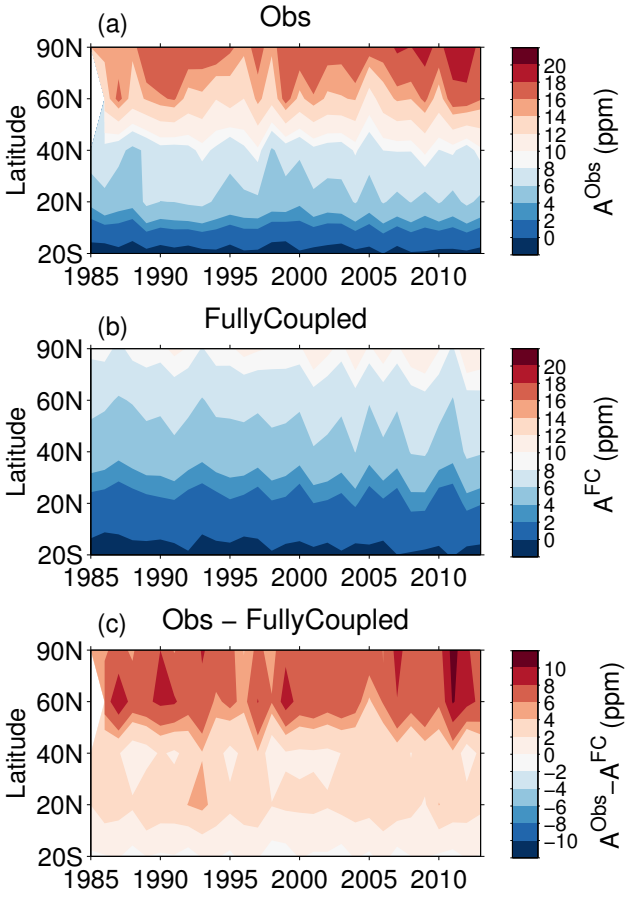

Figure 3. (a) Observed atmospheric CO_2 annual cycle amplitudes (A^{Obs}), (b) FullyCoupled atmospheric CO_2 annual cycle amplitudes (A^{FC}), and (c) the difference between A^{Obs} and A^{FC} during 1985–2013.

Biogeosciences Discuss., doi:10.5194/bg-2016-112, 2016
Manuscript under review for journal Biogeosciences
Published: 5 April 2016

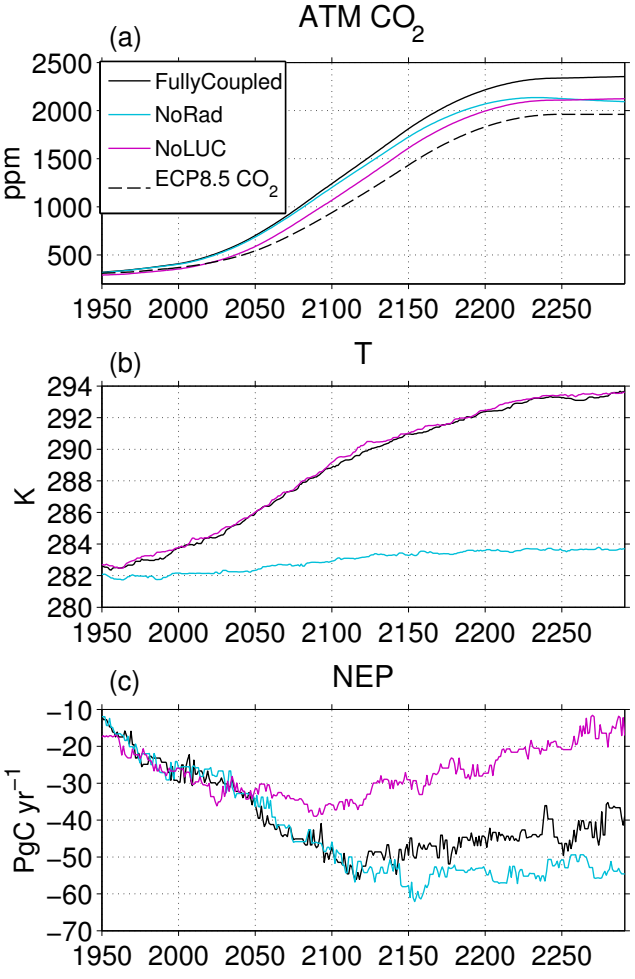

Figure 4. (a) Annual mean atmospheric CO_2, (b) annual mean bottom-level atmospheric T over land, and (c) annual total NEP averaged over the NH (0°–90°N) in the CESM FullyCoupled (solid black curves), NoRad (blue curves), and NoLUC (magenta curves) simulations. Negative NEP indicates net annual CO_2 uptake by the land surface. Values are filtered using a 10-year running median. The CO_2 mole fraction values in (a) result from the net contributions of land, ocean, and fossil fuel tracers calculated from NEE as described in Section 2.3, and differ from the atmospheric CO_2 mixing ratio that is prescribed according to the ECP8.5 scenario (dashed black curve).

Biogeosciences Discuss., doi:10.5194/bg-2016-112, 2016
Manuscript under review for journal Biogeosciences
Published: 5 April 2016

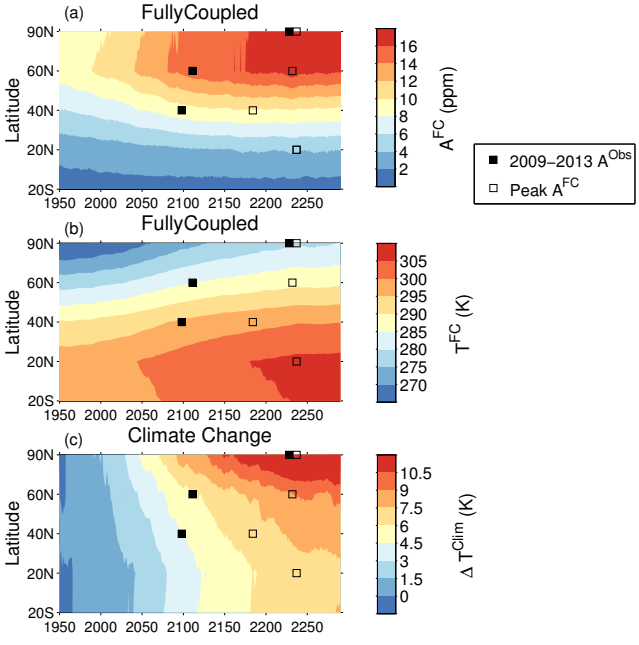

Figure 5. (a) 10-year moving averages of FullyCoupled atmospheric CO_2 annual cycle amplitude (A^{FC}) from 1950–1959 to 2280–2289. Black squares denote the decades in which the CESM reached observed CO_2 annual cycle amplitudes averaged over 2008–2013 in the NH high latitudes, NH subtropics, and SH tropics (Table 3). Open squares indicate the decades when peak amplitudes occurred in the midlatitudes and NH tropics, but did not reach present observed values. (b) Atmospheric temperatures over land in the FullyCoupled simulation (T^{FC}). (c) The change in atmospheric temperature with respect to the 1950–1959 mean caused by climate change (ΔT^{Clim}).

Biogeosciences Discuss., doi:10.5194/bg-2016-112, 2016
Manuscript under review for journal Biogeosciences
Published: 5 April 2016

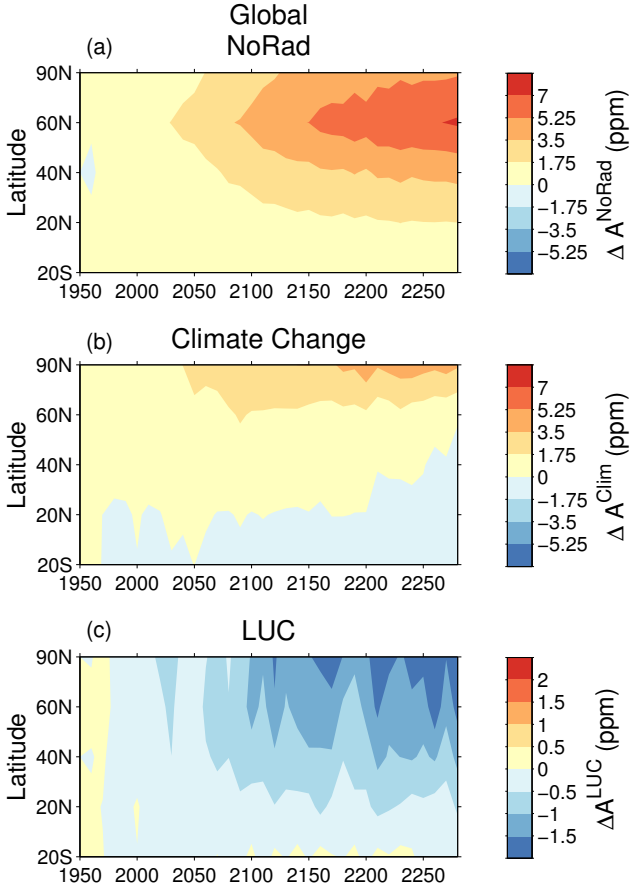

Figure 6. Changes in the decadal mean atmospheric CO_2 annual cycle amplitudes from present-day (1950–1959) values from (a) CO_2 fertilization and N-deposition (ΔA^{NoRad}), (b) Climate Change (ΔA^{Clim}), and (c) land use change (ΔA^{LUC}) from all land regions in each latitude bin.

Biogeosciences Discuss., doi:10.5194/bg-2016-112, 2016
Manuscript under review for journal Biogeosciences
Published: 5 April 2016

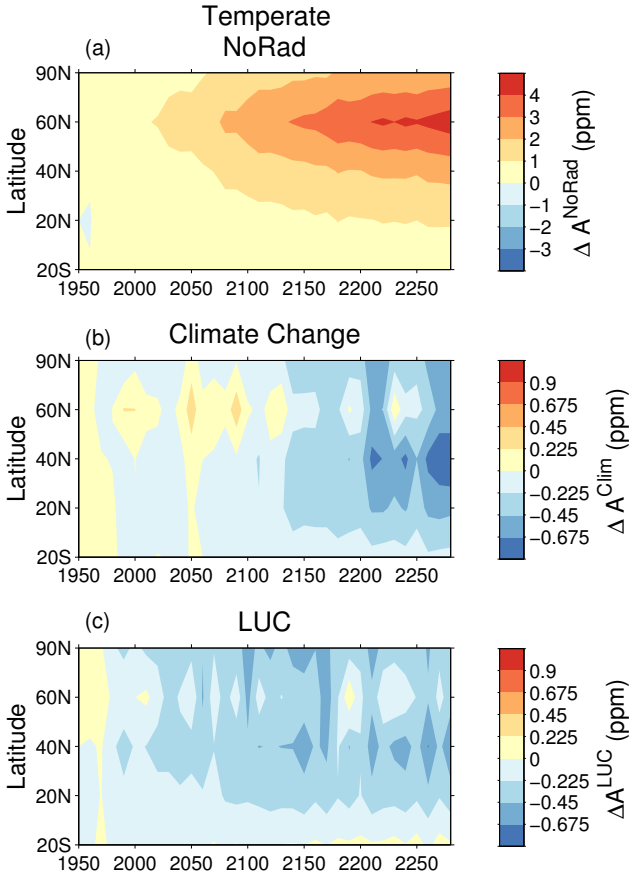

Figure 7. As in Fig. 6 but for CO_2 fertilization, N-deposition, climate change, and LUC from the NH temperate region.

Biogeosciences Discuss., doi:10.5194/bg-2016-112, 2016
Manuscript under review for journal Biogeosciences
Published: 5 April 2016

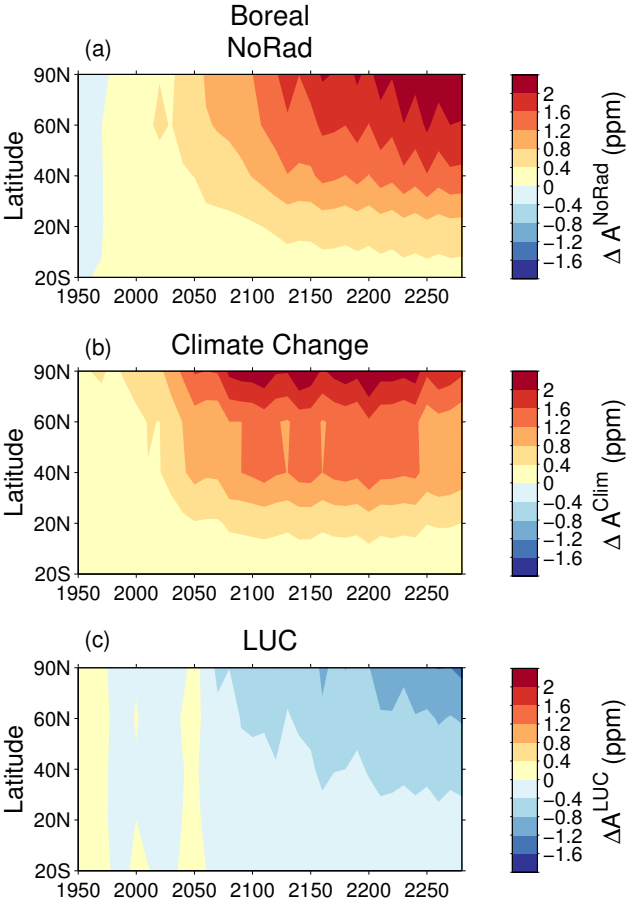

Figure 8. As in Fig. 6 but for CO_2 fertilization, N-deposition, climate change, and LUC from the NH boreal region.

Biogeosciences Discuss., doi:10.5194/bg-2016-112, 2016
Manuscript under review for journal Biogeosciences
Published: 5 April 2016

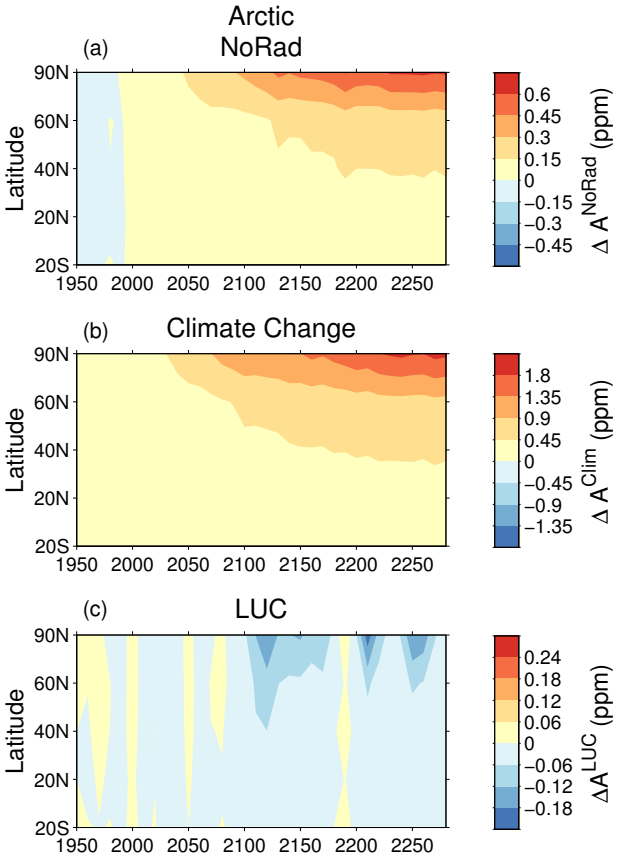

Figure 9. As in Fig. 6 but for CO_2 fertilization, N-deposition, climate change, and LUC from the Arctic.

Biogeosciences Discuss., doi:10.5194/bg-2016-112, 2016
Manuscript under review for journal Biogeosciences
Published: 5 April 2016

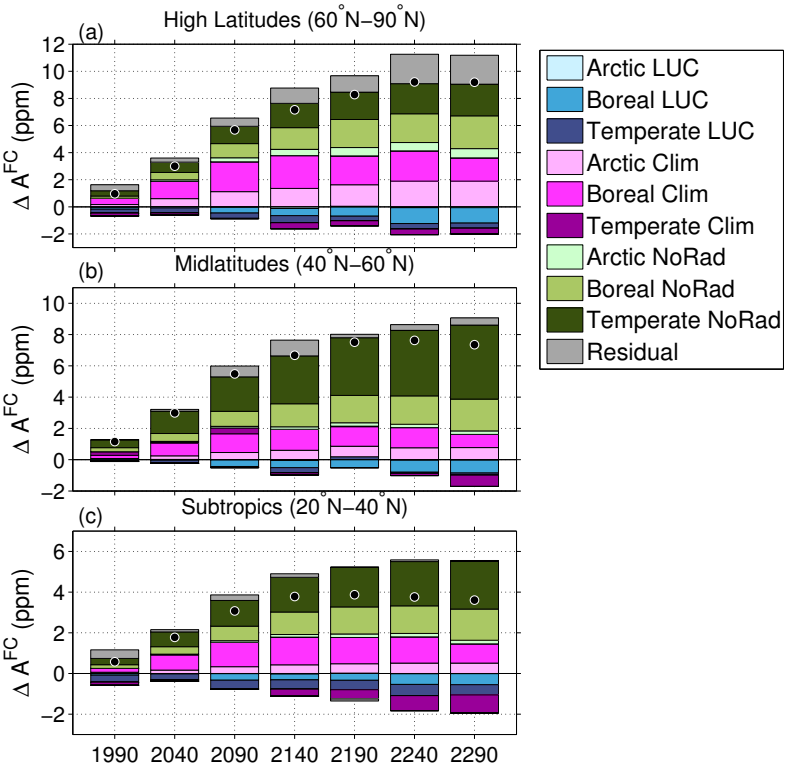

Figure 10. Contributions of Arctic, boreal, and temperate land use change (LUC), climate change (Clim), and combined CO_2 fertilization and N-deposition (NoRad) to the change in the FullyCoupled mean atmospheric CO_2 annual cycle amplitude from present-day (1950–1959) values (ΔA^{FC}) in the middle and final decades of the 21st, 22nd, and 23rd centuries over (a) the NH high latitudes, (b) the NH midlatitudes, and (c) the NH subtropics. Residual values are the sums of the contributions of LUC, climate change, CO_2 fertilization, and N-deposition in the subtropical, tropical, and SH GEOSChem land regions. Negative values indicate that the forcing decreased the atmospheric CO_2 annual cycle amplitude. Units are ppm.

Biogeosciences Discuss., doi:10.5194/bg-2016-112, 2016
Manuscript under review for journal Biogeosciences
Published: 5 April 2016

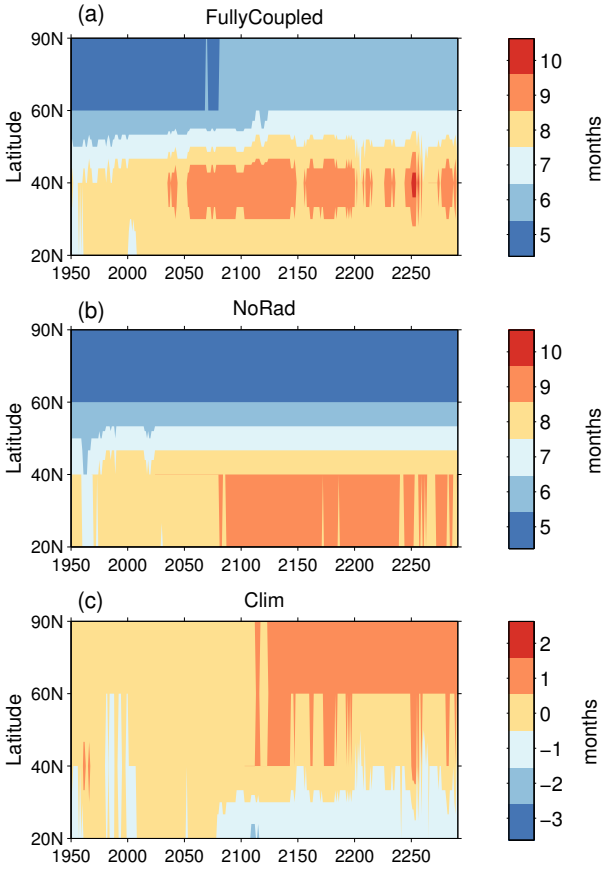

Figure 11. Growing season length (10-year running median of months with NEP < 0) in each latitude band in the (a) FullyCoupled, and (b) NoRad simulations. (c) The contribution of climate change to growing season length.

Biogeosciences Discuss., doi:10.5194/bg-2016-112, 2016
Manuscript under review for journal Biogeosciences
Published: 5 April 2016

Table 1. Region, station location, station ID, latitude, and longitude of CO_2 sample locations. Observations from bold stations were analyzed over the 1985–2013 period.

Region	Station Location	Station ID	Latitude	Longitude
Arctic	**Alert, Nunavut**	**ALT**	**82.45**	**297.49**
	Ny-Alesund, Svalbard	ZEP	78.90	11.90
	Barrow, Alaska	**BRW**	**71.30**	**203.40**
NH Midlatitudes	Baltic Sea	BAL	55.35	17.22
	Shemya Island, Alaska	**SHM**	**52.70**	**174.10**
	Hohenpeissenberg, Germany	HPB	47.80	11.02
	Hegyhatsal, Hungary	HUN	46.95	16.65
	Ulaan Uul, Mongolia	UUM	44.45	111.10
	Trinidad Head, California	THD	41.10	235.80
	Shangdianzi, China	SDZ	40.65	117.12
NH Subtropics	Tae-ahn Peninsula, Rep. Korea	TAP	36.70	126.10
	Mt. Waliguan, China	WLG	36.29	100.90
	Lampedusa, Italy	LMP	35.52	12.62
	Tudor Hill, Bermuda	BMW	32.30	295.10
	WIS Station, Negev Desert, Israel	WIS	29.97	35.06
	Izana, Tenerife, Canary Islands	IZO	28.31	343.50
	Sand Island, Midway, USA	**MID**	**28.21**	**182.62**
	Key Biscayne, Florida	**KEY**	**25.67**	**279.84**
	Lulin, Taiwan	LLN	23.47	120.87
NH Tropics	**Mauna Loa, Hawaii**	**MLO**	**19.50**	**204.42**
	Pacific Ocean (15°N)	POCN15	15.00	215.00
	Mariana Islands, Guam	**GMI**	**13.39**	**144.66**
	Ragged Point, Barabados	RPB	13.17	300.57
	Pacific Ocean (10°N)	PCON10	10.00	211.00
	Christmas Island, Rep. Kiribati	**CHR**	**1.700**	**202.85**
SH Tropics	Bukit Kototabang, Indonesia	BKT	-0.20	100.32
	Mahe Island, Seychelles	**SEY**	**-4.68**	**55.53**
	Maxaranguape, Brazil	NAT	-5.52	324.74
	Ascension Island, UK	**ASC**	**-7.97**	**345.60**
	Pacific Ocean (10°S)	POCS10	-10.00	199.00
	Tutuila, American Samoa	SMO	-14.25	189.44
	Pacific Ocean (20°S)	POCS20	-20.00	186.00
SH	Gobabeb, Namibia	NMB	-23.58	15.03
	Easter Island, Chile	**EIC**	**-27.16**	**250.57**
	Pacific Ocean (35°S)	POCS35	-35.00	180.00
	Cape Grim, Tasmania, Australia	**CGO**	**-40.68**	**144.69**
	Baring Head Station, NZ	BHD	-41.41	174.87
	Palmer Station, Antarctica	**PSA**	**-64.92**	**296.00**
	Syowa Station, Antarctica	SYO	-69.01	39.59
	Halley Station, Antarctica	**HBA**	**-75.61**	**333.79**
	South Pole, Antarctica	SPO	-89.90	335.20

Biogeosciences Discuss., doi:10.5194/bg-2016-112, 2016
Manuscript under review for journal Biogeosciences
Published: 5 April 2016

Table 2. GEOS-Chem regions shown in Fig. 1

Number	ID	Long Name
1	NBNA	Northern Boreal North America
2	SBNA	Southern Boreal North America
3	ETNA	Eastern Temperate North America
4	WTNA	Western Temperate North America
5	CNAM	Central America
6	AMZN	Amazon
7	EASA	Eastern South America
8	WESA	Western South America
9	EURO	Europe
10	SAME	Sahara and Middle East
11	MDAF	Mid Africa
12	AFRF	African Rainforest
13	SOAF	South Africa
14	EABA	Eastern Boreal Asia
15	WEBA	Western Boreal Asia
16	SOBA	Southern Boreal Asia
17	CNAS	Central Asia
18	SEAS	Southeast Asia
19	EQAS	Equatorial Asia
20	AUST	Australia
21	GNLD	Greenland
22	ATCA	Antarctica

Biogeosciences Discuss., doi:10.5194/bg-2016-112, 2016
Manuscript under review for journal Biogeosciences
Published: 5 April 2016

Table 3. Observed and FullyCoupled mean CO_2 annual cycle amplitudes, and corresponding decades when peak FullyCoupled amplitudes occurred in each latitude band shown in Fig. 3a.

Latitude	A^{Obs} (ppm) 1985–2013	A^{FC} (ppm) 1985–2013	Peak A^{FC} (ppm)	Center year of Decade of Peak A^{FC}
High Latitude	17.5	10.5	17.7	2241
Midlatitude	15.2	8.1	17.2	2236
Subtropics	9.3	6.7	10.0	2188
NH Tropics	6.7	3.8	4.4	2241
NH mean	10.1	6.3	9.9	2241

Biogeosciences Discuss., doi:10.5194/bg-2016-112, 2016
Manuscript under review for journal Biogeosciences
Published: 5 April 2016

Table 4. Cumulative changes in mean CO_2 annual cycle amplitudes (ppm) from the 1950–1959 baseline in the FullyCoupled simulation, and the contributions of non-radiative forcing (CO_2 fertilization and N-deposition), climate change, and LUC to the FullyCoupled amplitude changes averaged over the NH high latitudes, midlatitudes, subtropics, tropics, and the NH.

	FullyCoupled			NoRad			Climate Change			LUC		
High Latitudes	5.7	8.3	9.2	2.4	4.6	5.2	3.2	3.7	4.0	-0.9	-1.1	-1.6
Midlatitudes	5.5	7.5	7.4	3.5	6.3	7.4	1.9	1.2	-0.1	-0.6	-0.7	-1.3
Subtropics	3.1	3.9	3.6	2.0	3.6	4.1	1.0	0.3	-0.5	-0.8	-0.9	-0.9
NH Tropics	1.3	1.6	1.4	0.9	1.6	1.8	0.1	0	-0.4	-0.4	-0.3	-0.4
NH	3.1	4.1	4.1	2.0	3.5	4.0	1.1	0.6	0.1	-0.6	-0.7	-0.9
Year	2100	2200	2300	2100	2200	2300	2100	2200	2300	2100	2200	2300